PAPER

The inter-ELM tungsten erosion profile in DIII-D H-mode discharges and benchmarking with ERO+OEDGE modeling

To cite this article: T. Abrams *et al* 2017 *Nucl. Fusion* **57** 056034

IOP Publishing | International Atomic Energy Agency Nuclear Fusion

Nucl. Fusion **57** (2017) 056034 (10pp) https://doi.org/10.1088/1741-4326/aa66b2

The inter-ELM tungsten erosion profile in DIII-D H-mode discharges and benchmarking with ERO+OEDGE modeling

T. Abrams[1], R. Ding[2], H.Y. Guo[1], D.M. Thomas[1], C.P. Chrobak[3], D.L. Rudakov[3], A.G. McLean[4], E.A. Unterberg[5], A.R. Briesemeister[5], P.C. Stangeby[6], J.D. Elder[6], W.R. Wampler[7] and J.G. Watkins[8]

[1] General Atomics, San Diego, CA 92186-5608, United States of America
[2] Oak Ridge Associated Universities, Oak Ridge, TN 37830, United States of America
[3] University of California San Diego, San Diego, CA, United States of America
[4] Lawrence Livermore National Laboratory, Livermore, CA 94550, United States of America
[5] Oak Ridge National Laboratory, Oak Ridge, TN 37831, United States of America
[6] University of Toronto Institute for Aerospace Studies, Toronto, M3H 5T6, Canada
[7] Sandia National Laboratories, Albuquerque, NM 87185, United States of America
[8] Sandia National Laboratories, Livermore, CA 94551, United States of America

E-mail: abramst@fusion.gat.com

Received 20 September 2016, revised 2 March 2017
Accepted for publication 14 March 2017
Published 3 April 2017

Abstract

It is important to develop a predictive capability for the tungsten source rate near the strike points during H-mode operation in ITER and beyond. H-mode deuterium plasma exposures were performed on W-coated graphite and molybdenum substrates in the DIII-D divertor using DiMES. The W-I 400.9 nm spectral line was monitored by fast filtered diagnostics cross calibrated via a high-resolution spectrometer to resolve inter-ELM W erosion. The effective ionization/photon (S/XB) was calibrated using a unique method developed on DIII-D based on surface analysis. Inferred S/XB values agree with an existing empirical scaling at low electron density (n_e) but diverge at higher densities, consistent with recent ADAS atomic physics modeling results. Edge modeling of the inter-ELM phase is conducted via OEDGE utilizing the new capability for charge-state resolved carbon impurity fluxes. ERO modeling is performed with the calculated main ion and impurity plasma background from OEDGE. ERO results demonstrate the importance a mixed-material surface model in the interpretation of W sourcing measurements. It is demonstrated that measured inter-ELM W erosion rates can be well explained by C→W sputtering only if a realistic mixed material model is incorporated.

Keywords: DIII-D, DiMES, tungsten, erosion, sputtering, ERO modeling

(Some figures may appear in colour only in the online journal)

1. Introduction

The ITER divertor will be composed of tungsten plasma facing components (PFCs) in order to mitigate the detrimental effects of high heat and particle fluxes expected during H-mode operation and minimize tritium retention [1]. Despite the low expected erosion rate of W under ITER divertor particle fluxes, even relatively small core W impurity concentrations are unacceptable in ITER and beyond from the standpoint of fuel dilution, plasma conduction, heating efficiency, and avoiding radiative collapse. It has been proposed to operate ITER and future devices with a partially detached divertor in order to mitigate these W erosion fluxes but compatibility of partial detachment with high plasma confinement

regimes remains an active field of study. It becomes necessary to develop a physics understanding for the temporally and spatially resolved high-Z divertor source under different edge plasma conditions. Previous work on the JET-ITER-like wall (ILW) [2, 3] and in ASDEX-U [4] has asserted that spatially-averaged W erosion between edge localized modes (ELMs) in H-mode is roughly consistent with the rates predicted by impurity-induced W sputtering. The dominant plasma impurity is beryllium in the JET-ILW case and C in the ASDEX-U case.

This paper represents a refinement of the measurement and modeling techniques used in previous work through highly spatially resolved measurements of the inter-ELM W erosion profile and the first benchmarking of these results against the OEDGE and ERO codes. For this work, spectroscopic measurements of the W erosion source in the DIII-D divertor were conducted with very high spatial resolution (~0.8 mm). First, calibration of the effective S/XB ratio for the WI 400.9 nm line using a unique surface analysis technique to quantify the gross erosion rate of W for constant L-mode plasmas is presented. Inferred S/XB values compare favorably with the empirical scaling presented in [2] and atomic data and analysis structure (ADAS) calculations [5, 6] at low densities ($n_e < 10^{13}$ cm^{-3}) but a discrepancy is discovered between measurement and the empirical scaling at higher densities.

Next, inter-ELM W erosion measurements during a broad variety of H-mode plasma conditions are discussed. It is shown that a simple analytic model of impurity-induced W sputtering by C impurities cannot closely replicate experimental measurements. To arrive at a better physics understanding, the spatially-resolved W erosion profile for a well diagnosed, attached H-mode plasma condition in DIII-D is benchmarked against code models. The OEDGE code was used to develop an inter-ELM plasma background using the new capability for charge state-resolved carbon impurity fluxes and impact energy distributions [7], which is used as input into the ERO 3D Monte Carlo plasma materials interaction (PMI) code [8]. The ERO code has been previously used to benchmark the gross and net erosion rate of various materials in tokamaks [9–11], with varying degrees of success. In this study, the inter-ELM W erosion profile calculated by ERO+OEDGE agrees well with experimental measurements without the need to introduce free parameters into the plasma surface interactions, the first step towards predictive capability.

2. Materials and methods

2.1. DiMES

Plasma exposures of W-coated PFCs were conducted using the DIII-D divertor materials evaluation system (DiMES), a well-established tool for studying plasma material interactions in the DIII-D divertor [12]. DiMES allows for the insertion, exposure, and removal of circular, ~4.8 cm material surfaces flush with the divertor floor for as short as a single plasma discharge. The location of DiMES within the DIII-D vessel is shown in figure 1. W coatings were applied to DiMES caps via magnetron sputtering at Sandia National Laboratory or via

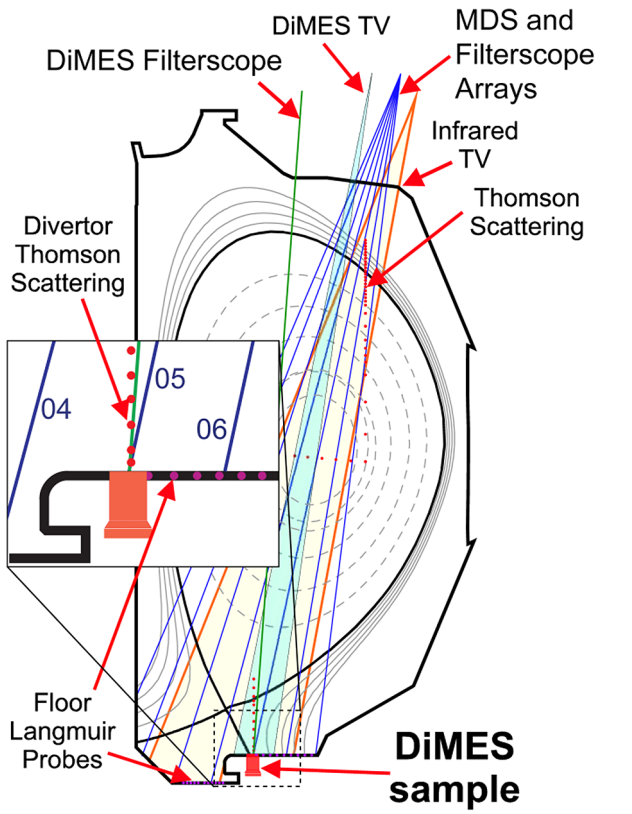

Figure 1. Poloidal cross section of the DIII-D vessel depicting the edge plasma and spectroscopic diagnostics utilized in this series of DiMES experiments. Inset: a magnified version of the divertor/DiMES region, indicating the position of the Langmuir probes, divertor Thomson scattering chords and MDS/filterscope chords.

evaporative deposition at Oak Ridge National Laboratory. W coatings ranged from 40 nm to 500 nm in thickness and were applied to either graphite or titanium–zirconium–molybdenum (TZM) molybdenum alloy substrates depending on the particular experimental application; details are provided in the ensuing sections. For L-mode experiments designed to measure the S/XB ratio of the WI 400.9 nm line (section 3), masks were applied to the W-coated samples to measure both gross and net erosion; see [13] and section 3 for details on this technique. All samples exposed to H-mode plasma conditions (sections 4 and 5) were completely coated with tungsten.

2.2. Edge spectroscopic and plasma diagnosis

In situ measurements of the gross erosion rate of W were conducted by measuring the spectral intensity (photons cm^{-1} s^{-1}) of the WI 400.9 nm line; similar techniques have been used on other devices [2, 4, 14]. Spectroscopic diagnosis of the W erosion rate in H-mode plasmas is necessary to distinguish W erosion due to ELMs from the source between ELMs. The view chords of the edge spectroscopy diagnostic suite for the DIII-D lower divertor are shown in figure 1.

The multichordal divertor spectrometer (MDS), a high spectral resolution Czerny-Turner spectrometer [15], provides spectrally resolved information on the WI 400.9 line intensity with an integration time of 200–500 ms. Geometric corrections to the WI emission intensity were performed because

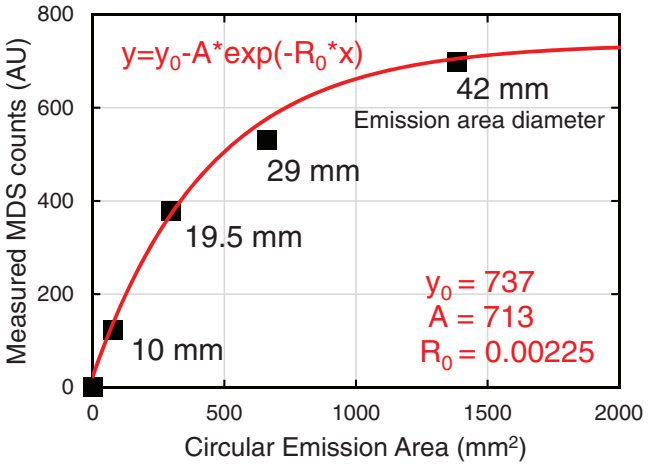

Figure 2. Measured emission intensity on the MDS relative to the diameter of an apertured, uniform circular light source. An exponential fit to these data are also overlaid, with fitting parameters listed.

the size of the W-coated regions on these DiMES samples was smaller than the spot size of the MDS viewing chord. *In situ* calibration of the appropriate geometric correction factor was performed using a uniform light source centered at the DiMES location and covering the source with apertures of varying diameters. In figure 2, the measured intensity of the light source is plotted against the total emission area of the apertured light source. It is evident that the MDS viewing spot is not in perfect focus because the measured intensity does not increase linearly with emission area before 'plateauing' at a constant value, but the emission intensity fits reasonably well with an exponential decay, also shown in figure 2. The geometric correction factor is obtained by calculating the fraction of light emission originating from inside the W-coated region of the DiMES sample. For the DiMES Type A sample (figure 3) the resulting geometric correction factor is ~5.85 and for the Type B sample this factor is ~3.15.

DiMES is imaged by a CCD-based camera (PCO Pixelfly VGA 200/205) with an exposure time of 10 ms, 100 Hz framing rate, and ~0.8 mm spatial resolution. A band-pass filter with a center wavelength of 400.9 nm and full width half maximum (FWHM) of ~1.5 nm is placed within the optical pathway to filter the WI 400.9 nm line. Due to the relatively weak intensity of this spectral line, it is necessary to perform a background subtraction to eliminate the contribution of continuum emission (visible bremsstrahlung) and contaminant lines within the spectral transmission range of the band-pass filter. This analysis is performed by subtracting the measured count rates ~3 cm offset, in both the upstream and downstream direction, but at the same radial position as the DiMES sample:

$$I_{\mathrm{WI}} = \frac{A}{\Delta t_{\mathrm{exp}}}\left[\frac{C_{\mathrm{W}}}{1+R_{\mathrm{W}}} - \frac{0.5(C_{\mathrm{g,up}}+C_{\mathrm{g,down}})}{1+R_{\mathrm{g}}}\right]. \quad (1)$$

Here I_{WI} is the absolute intensity of the WI 400.9 nm line (photons cm^{-2} s^{-1}), Δt_{exp} is the camera exposure time (10 ms), and A is an absolute calibration factor (photons cm^{-2} sr^{-1} pixel^{-1}). A cross-check against the MDS spectrometer was performed and the intensity values were in good agreement (within 20%). C_{W} and $C_{\mathrm{g,up}}/C_{\mathrm{g,down}}$ are the counts/pixel measured by the camera on the W DiMES sample and on the graphite tiles ~3 cm upstream/downstream of the DiMES probe. R_{W} and R_{g} are empirical coefficients representing the effective reflectivity of the tungsten and graphite surfaces. A constant value of $R_{\mathrm{g}} = 0.1$ was assumed based on post-mortem measurements conducted on graphite DiMES samples with a reflection probe. The value of R_{W} was calibrated such that $I_{\mathrm{WI}} = 0$ during the initial limiter configuration phase of each plasma discharge before the outer strike point (OSP) is placed on DiMES, i.e. the entire filtered camera signal is assumed to be due to background emission, rather than W erosion, during this phase. The typical value of R_{W} obtained was 0.2–0.25, assumed not to be strongly dependent on surface modifications and impurity accumulation on the time scale of one discharge.

An array of fast photomultiplier tube (PMT)-based diagnostics (filterscopes) [16] view the DIII-D divertor region along approximately the same chords as the MDS, but at a different toroidal location. A new filterscope view was also developed for this study that directly views the DiMES surface with a ~2.5 cm spot size, effectively the same viewing spot as the DiMES-viewing chord of the MDS. This enables measurement of the WI 400.9 nm spectral line on fast time scales (20 μs) and absolute WI intensities via cross calibration with MDS. A novel background subtraction technique was developed using a fiber optic beam splitter to separate the WI intensity from the continuum background intensity. This technique does not require the assumption of a constant continuum background level throughout one entire plasma discharge, as utilized in previous work [3]. Details of this new technique are presented in [17].

Characterization of the electron temperature and density profiles at the DiMES location are obtained via Langmuir probes and the lowest vertical chord of the divertor Thomson scattering (DTS) diagnostic (figure 1, inset). Agreement is typically fairly good between these two diagnostics in attached plasma regimes [18]. The Langmuir probes (pink circles in figure 1, inset) are generally incapable of measuring divertor electron temperatures lower than ~5 eV due to fast plasma fluctuations strongly perturbing the *I–V* characteristic so for low temperature measurements, DTS is solely used. Slow strike point sweeping (~2 cm s^{-1}) is used to build high-resolution edge plasma profiles of divertor n_e and T_e. It has been demonstrated on DIII-D that the OSP can be swept over nearly the entire divertor floor without appreciably changing plasma conditions relative to the OSP position [19].

3. Spectroscopic analysis of the WI S/XB coefficients

The ionization/photon, or S/XB, method provides a direct proportionality factor between photon emission intensity and atomic ionization rates:

$$\Gamma_Z = 4\pi I_{Z,\mathrm{tot}}\frac{S}{XB}, \quad (2)$$

where Γ_Z is the ionization flux (atoms cm^{-2} s^{-1}), assumed equal to the gross material influx, and $I_{Z,\mathrm{tot}}$ is the total photon emission rate (photons cm^{-2} s^{-1} sr^{-1}) for a given spectral

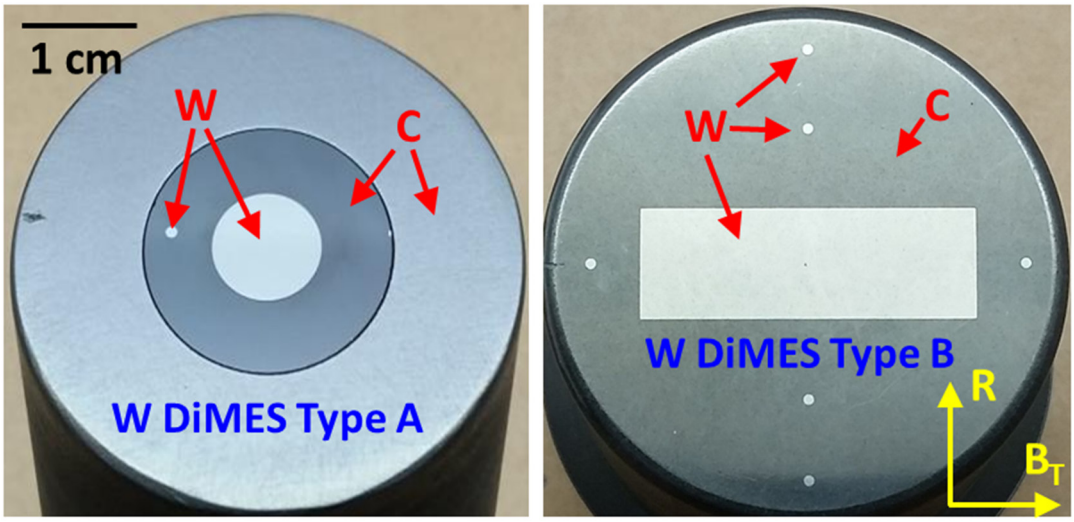

Figure 3. Photographs of the two types of DiMES samples used for measurements of the WI 400.9 nm S/XB coefficient. Sample Type A contains a 1 mm and 1 cm diameter W spot. Sample B contains a 1 × 3 cm W stripe and six 1 mm diameter W spots.

line. Note that equation (2) makes several simplifying atomic physics assumptions to facilitate comparisons with experimental measurements. Additional context on the application of the S/XB method, as well as extensive calculations and measurements of S/XB coefficients for many fusion-relevant atomic species, are provided in [20]. For measuring the erosion rate of W, the 400.9 nm WI line, the brightest neutral W line in the visible spectral range, is typically used [2, 4] and some measurements on other lines have also been performed [21]. It was verified that the spectroscopy diagnostics described in section 2 were well calibrated by comparing measurements of the WI 400.9 nm S/XB coefficient with the existing empirical scaling from previous devices [2]. This study also provided an opportunity to expand the existing data set to a larger range of electron densities and to compare measurements with recently available theoretical values derived using the ADAS collisional radiative model [5].

The procedure for measurements of the WI 400.9 nm S/XB coefficient was as follows. Two types (Type A and Type B) W-coated graphite DiMES samples were prepared as described in section 2.1 and depicted in figure 3. Both types of samples enabled the measurement of gross W erosion by comparing the absolute W areal density (W atoms cm^{-2}) on the 1 mm diameter W spots before and after plasma exposure using Rutherford backscattering spectrometry (RBS). Details on this technique have been previously published [13]. The large 1 cm diameter W circle on the Type A sample and 1 × 3 cm stripe on the Type B sample provided sufficiently large spectroscopic signals of the WI 400.9 nm line. Two samples of Type A and one of Type B were exposed to a series of 3–4 constant L-mode plasmas. The material erosion rate is assumed to be constant during the 3 s interval on each shot in which the OSP is fixed ~2 cm inboard of the DiMES center. The plasma density and temperature conditions for each set of exposures, obtained via DTS, are displayed in figure 4.

Equation (2) implies that the inferred S/XB coefficient for each set of plasma conditions is equal to the average gross erosion rate of W (measured via RBS) divided by the average WI 400.9 nm emission intensity (obtained via the MDS). The inferred values for the WI 400.9 nm S/XB ratio are plotted as a function of T_e in figure 4. Error in these measurements stems primarily from uncertainty in the absolute calibration of the MDS and the geometric corrections to the WI emission intensity, as discussed in section 2.2. The existing empirical experimental scaling [1] is also shown. The DiMES data points acquired at $n_e \sim 10^{13}$ cm^{-3} show good agreement with this scaling, but a discrepancy is observed with the one data point acquired at a higher electron density (~5×10^{13} cm^{-3}). No data used in the empirical scaling were obtained at densities higher than 10^{13} cm^{-3} so this new result may suggest a previously unobserved density dependence for the WI 400.9 nm S/XB coefficient for $n_e > 10^{13}$ cm^{-3}.

This result is compared with two sets of theoretical calculations [5, 22]. The calculations in [22] have a free parameter T_W to model the underlying distribution of low-lying atomic energy levels as a Boltzmann distribution. These calculations appear to over-estimate the measured values by approximately a factor of 2, except for the high-density DiMES measurement which agrees reasonably well with a T_W value of 0.3–2.0 eV. The dataset described in [5] utilizes the ADAS collisional-radiative model. The ADAS data show a similar dependence on T_e to experimentally measured values and also displays a strong dependence on n_e above 10^{13} cm^{-3}. This is consistent with the measurement conducted via DiMES at high density. A more systematic evaluation of the dependence of WI S/XB coefficient on electron density for multiple WI spectral lines should be conducted in the future, but no additional measurements were available for this paper.

These theoretical calculations can also be tested by line ratio analysis. It is evident from equation (2) that the measured intensity ratio for two given spectral lines is equal to the reciprocal ratio of their respective S/XB coefficients. In a separate experiment, both the WI 400.9 nm line and the WI 429.4 nm line were monitored by the MDS during repeat, consecutive H-mode W DiMES exposures. Because the MDS did does provide sufficient time resolution (200 ms) in these discharges to

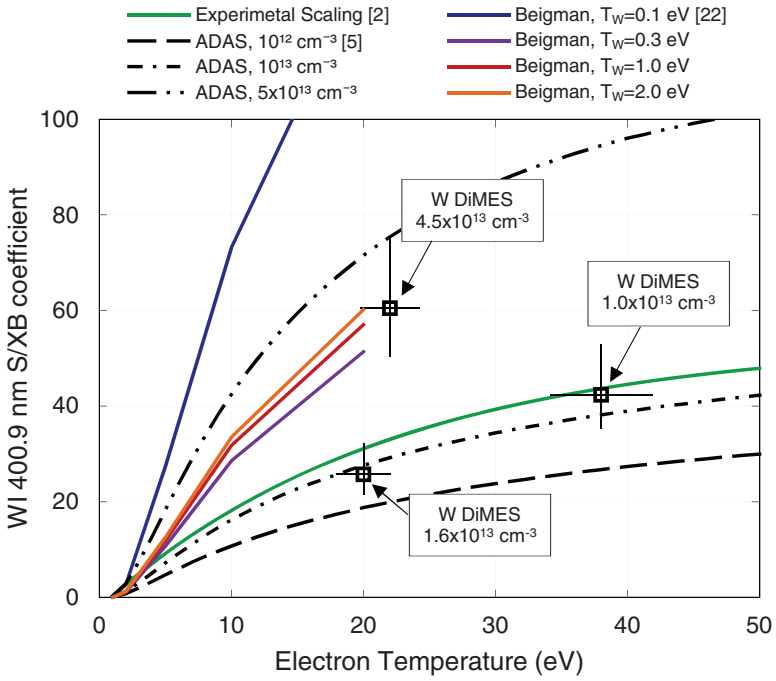

Figure 4. Measurements and theoretical values for the WI 400.9 nm S/XB coefficient plotted as a function of electron temperature. Measurements conducted via DiMES are plotted as square symbols. An empirical scaling based on previous experimental data [2] is also plotted, as well as two sets of theoretical calculations [5, 22].

resolve ELMs there is an implicit averaging of intra-ELM and inter-ELM divertor plasma conditions. The absolute intensity of each WI spectral line is plotted against the inter-ELM edge plasma electron temperature at the DiMES location (obtained via DTS) in figure 5(*a*). Divertor density varied identically with T_e during these two repeat discharges so it is considered a reasonable assumption that the D and C ion fluxes to the W surface, and thus the Γ_Z term in equation (2), varied similarly with T_e in both cases. A similar relationship between intensity and T_e is observed for both WI lines, although the functionality is somewhat more pronounced for the 400.9 nm line. A parabolic fit is overlaid for both lines. No justification is provided for this particular functional form except that it fits the available experimental data reasonably well.

The ratio of the parabolic fits to the 400.9 nm and 429.4 nm spectral line intensities is plotted in figure 5(*b*). This ratio ranges from ~0.6 to ~0.85, close to previous measurements on TEXTOR of 0.7–1.0 [22], although the functional dependence of this ratio on T_e was not provided in this previous study. Also plotted in figure 5(*b*) are the reciprocal ratios of the WI S/XB coefficients from the two available theoretical datasets. The reciprocal S/XB ratio predicted by ADAS [5] displays virtually no density dependence and thus is plotted as a single curve. The ratio predicted by Beigman *et al* [22] is effectively constant for $T_W \geqslant 0.3$ eV but drops slightly for $T_W = 0.1$ eV, so two cases are plotted. Comparing these calculations to experimental measurements, a fairly flat functional dependence of the line ratio to electron temperature is observed in all cases, although the measurements show slightly more variation with T_e than theory. The measured line ratio is lower by about a factor of 2 relative to the theoretical values. It is noted by Beigman *et al* that such discrepancies could result from configuration mixing or strong cascade effects not properly accounted for in the modeling. The discrepancy between measurements and ADAS values may imply the relative populations of the metastable states require adjustment. Preliminary efforts to correct the neutral W metastable fractions are in progress but are beyond the scope of this paper. In summary, theoretical datasets make simplifying assumptions concerning the atomic structure of the W atom so agreement with experiment may be inconsistent. Further discussion of atomics physics modeling of neutral tungsten is provided in section 6.

4. Inter-ELM gross erosion rates of W in H-mode

For the purposes of studying the inter-ELM W erosion source in DIII-D H-mode plasma conditions, we analyze a series of H-mode discharges where divertor n_e and T_e were varied by sweeping the OSP relative to DiMES. In some discharges additional low field side D_2 gas fueling was added, resulting in divertor plasma cooling and increased electron density. WI emission obtained via the DiMES-viewing filterscope chord (figure 1) was background-subtracted and absolutely calibrated as described in section 2.2 and in [17]. ELM filtering is performed using edge detection analysis on a D_α lower divertor filterscope chord (fs06 in figure 1). WI emission from 50% to 99% of the inter-ELM cycle, chosen in order to obtain sufficient plasma n_e and T_e measurement statistics via DTS, is averaged in 200 ms time increments. The DTS laser fires with 50 Hz frequency, typically resulting in 5–6 useable data points in a 200 ms binning period once ELMs and fits with poor statistics are removed.

For the purpose of comparison with previous data sets, we use the existing experimental scaling for the WI 400.9 nm S/XB coefficient [2], with the caveat that this may underestimate the S/XB ratio at electron densities significantly higher

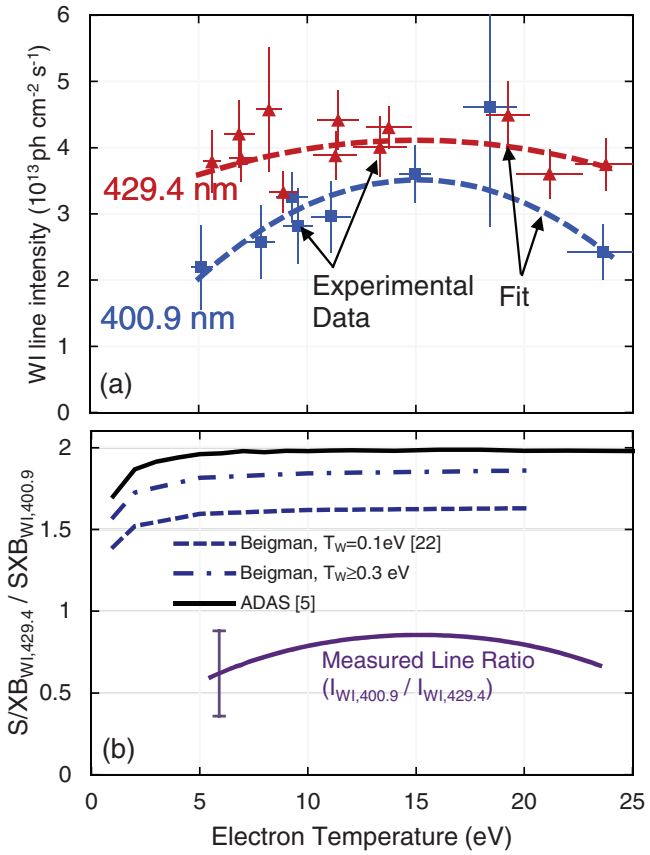

Figure 5. (*a*) The measured absolute intensity of two WI spectral lines versus divertor electron temperature, with parabolic fits overlaid. (*b*) Ratio of the parabolic fits $I_{WI,400.9}/I_{WI,429.4}$ plotted above, in addition to the reciprocal ratio of S/XB coefficients for these two spectral lines from theoretical calculations [5, 22].

than 10^{13} cm^{-3}, as described in section 3. W erosion flux measurements are normalized to the incoming deuterium ion flux $\Gamma_{D+} = n_e\left(\frac{T_e + T_i}{m_i}\right)^{1/2}$ where m_i is the deuteron ion mass and n_e,T_e are obtained via DTS as discussed above. The plasma is assumed sufficiently collisional such that $T_e = T_i$. C and W impurities are present in the divertor plasma in only trace amounts (<1%) and thus corrections to the formula for Γ_{D+} given above are not necessary. It has been well established [2, 4] that inter-ELM high-Z erosion is dominated by impurity-induced sputtering so this normalization results in an 'effective' erosion yield only. Further evidence for this assertion is discussed in section 5 for inter-ELM H-mode conditions and in [9, 23] for L-mode conditions.

The normalized tungsten erosion yield Γ_W/Γ_{D+} is plotted as a function of T_e (the average of the inter-ELM DTS measurements in each binning window) in figure 6. Inter-ELM divertor electron densities range from 0.1–5 × 10^{14} cm^{-3} for these measurements. As mentioned above, each data point represents the average of 200 ms of approximately constant inter-ELM plasma conditions. A logarithmic-type trend is evident in the effective W erosion yield, similar to previous datasets [2]. Also plotted in figure 6 are the effective C→W sputtering yields calculated via SDTrimSP [24] for C^{3+} ion flux fractions of 1%, 2%, and 4% relative to the deuterium ion flux, as well as a 0.5%

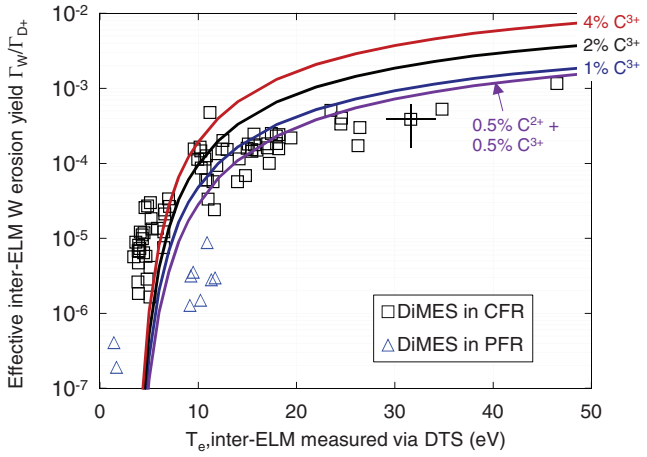

Figure 6. Inferred spectroscopic measurements of the effective inter-ELM W erosion yield Γ_W/Γ_{D+} plotted as a function of T_e measured via DTS 1 cm above the DiMES surface. Exposures where DiMES was in the common flux region (CFR) are shown in squares and where DiMES was in the private flux region (PFR) are shown with triangles. Also shown are the theoretical C→W sputtering yields obtained via SDTrimSP for several fixed concentrations of C^{2+} and/or C^{3+} (solid lines).

C^{2+} and 0.5% C^{3+} flux fraction. For these calculations, the C ions are assumed to have a Maxwellian energy distribution of temperature T_e plus an additional energy of $3ZT_e$ due to sheath acceleration, with a uniform ion impact angle of 45° relative to surface normal. The dynamic TRIDYN portion of the code has been disabled for these studies. These results are qualitatively consistent with the picture of C→W impurity sputtering characterized by a cut-off low ion impact energies, an exponential increase in sputtering yield with increasing energy, and a plateau forming at C impact energies of several hundred eV.

However, it is also clear that a single C flux fraction without taking into account the C/W mixed material and prompt processes (e.g. W→W self-sputtering via W prompt redeposition) do not provide a complete picture of the physics of inter-ELM W sputtering in the DIII-D divertor. Generally the SDTrimSP model over-predicts the W erosion yield, particularly at high temperatures. This motivates the development of more careful physics models of the spatially resolved W erosion profile using high-resolution 3D Monte Carlo simulations that include a more realistic model of the impurity plasma background as well as non-linear effects of C/W material mixing and prompt processes. Such simulations are described in the next section.

5. Simulating the inter-ELM W erosion profile via ERO+OEDGE

5.1. OEDGE modeling

In order to benchmark PMI models of inter-ELM W erosion, the inferred W erosion profile from DIII-D discharge 163216 was selected for analysis due to the existence of a well-diagnosed, large inter-ELM W erosion rate and well-characterized edge plasma parameters. An edge plasma background solution for this discharge was developed with the OEDGE code

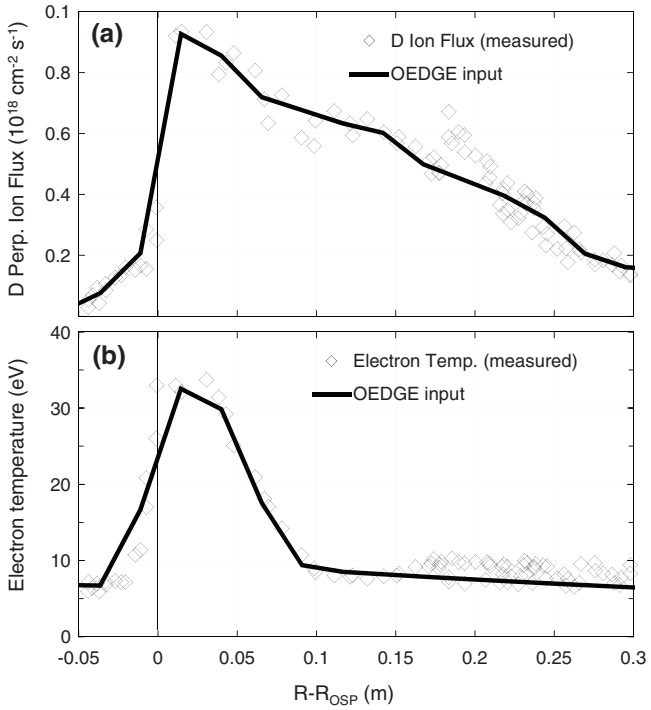

Figure 7. Symbols: profiles of (*a*) divertor ion saturation flux and (*b*) divertor electron temperature, obtained via Langmuir probe measurements, near the OSP for discharge 163215 studied in this section. Solid lines: smoothed curves used as input into OEDGE simulation.

[7, 23] using the process of empirical plasma reconstruction. Langmuir probe measurements of T_e and ion saturation current (J_{sat}) from a repeat discharge (163215) with a longer OSP sweep over the lower outer divertor (figure 1) were used as the target plasma conditions. Inferred T_e and J_{sat} profiles are shown in figure 7 with the smoothed OEDGE inputs overlaid. The onion skin model (OSM) plasma solver portion of OEDGE calculates plasma conditions (n_e, T_e, T_i, parallel plasma flow, parallel electric field) along field lines. This solution is run iteratively with the EIRENE code, which calculates the neutral densities and energy loss terms, until a specified convergence criterion is met. The impurity tracking portion of OEDGE (DIVIMP) calculates carbon impurity production, transport, and deposition. These calculations result in a carbon flux and average impact energy profile with high spatial resolution at the DiMES location (figure 8). Carbon charge states $Z = 2$ and $Z = 3$ are dominant and contribute approximately equally to the impurity flux to the surface. The contribution from other charge states is negligible.

The quality of the OEDGE plasma solution was benchmarked by comparing predicted inter-ELM D_α (656 nm) and CIII (465 nm) line emission profiles near OSP with experimental data. The OEDGE code is capable of generating synthetic diagnostic emission profiles that account for the geometric viewing characteristics (i.e. the finite solid angle of a viewing chord) of the DIII-D divertor-viewing filterscope channels. The corresponding experimental measurements are obtained via binning inter-ELM photon fluxes in 5 ms increments from filterscope views fs05, centered at the same major radius as the W DiMES sample but at a different toroidal location, and fs06, located ~11 cm outboard of DiMES (figure 1).

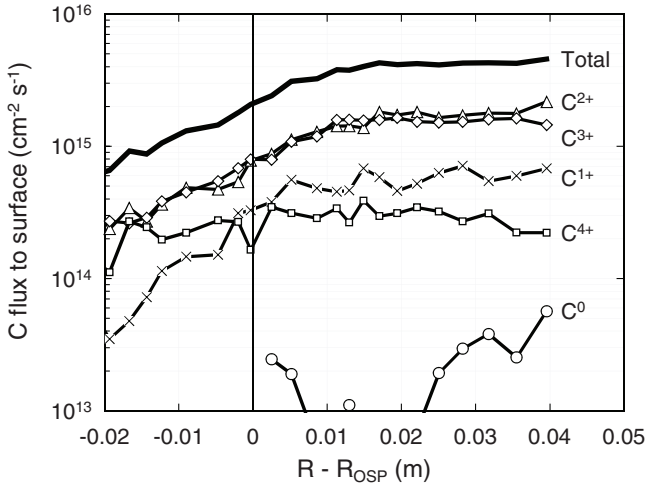

Figure 8. Calculated C impurity fluxes near the DIII-D OSP as a function of radial position for discharge 163216 using OEDGE. C^{2+} and C^{3+} represent the dominant C charge states.

Spectroscopic information was obtained during repeat discharge 163215 with a long OSP sweep across the divertor surface. It was observed that the CIII emission rates from fs06 are systematically higher by a factor of ~2 than the other four CIII filterscope views (fs02–fs05) in the DIII-D lower divertor. It is believed that this discrepancy is due to contamination of the filter bandpass region (463.5–467.5 nm) with other impurity emission lines, although spectrally resolved emission rates were not available in this wavelength range during this experiment. A compensation factor of 0.5 was applied to the absolute photon fluxes from the fs06 CIII viewing chord. Measurements of additional D and C spectral lines were not available because the fs06 filterscope view contains only CIII, D_α, and He I/II bandpass filters. No appreciable divertor He content was present in the studied discharges.

The measured D_α and CIII spatially-resolved line emission profiles from the fs05 and fs06 viewing channels are shown in figure 9. The geometric viewing characteristics of the fs05 and fs06 viewing chords are identical; they differ only in absolute radial position, so the OEDGE calculation is overlaid as a single curve which depends only on R–R_{OSP}. Generally correspondence is observed within 50% between measured D_α and CIII photon emission rates and OEDGE predictions. Similar matches between measured line radiation profiles and those computed by OEDGE have previously been achieved on DIII-D during ohmic L-mode experiments [23]. Given the uncertainties associated with ELMs and other divertor plasma fluctuations in H-mode discharges, the data in figure 9 is considered reasonable agreement. In particular, in the range of -0.02 m $< R$–$R_{OSP} < 0.05$ cm of prime interest for benchmarking ERO simulations, the OEDGE calculations match rather well with spectroscopic measurements, although the C^{2+} concentration in the divertor plasma may be slightly underestimated.

5.2. ERO modeling

The main ion and impurity plasma profiles calculated via OEDGE are used as input into the 3D Monte Carlo code ERO (version 1.0). The first portion of this code calculates

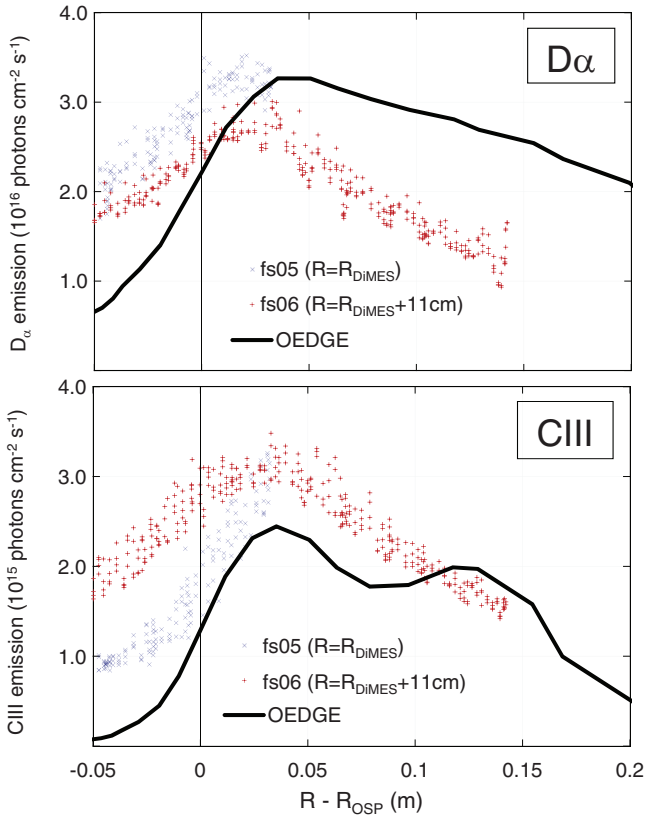

Figure 9. Solid lines: Calculated D_α (656 nm) and CIII (465 nm) inter-ELM photon fluxes near the DIII-D OSP as a function of radial position for discharges 163215-6 using OEDGE. Symbols: Experimental measurements of the D_α and CIII photon fluxes obtained via filterscope diagnostics. Generally reasonable agreement is observed between OEDGE and experiment.

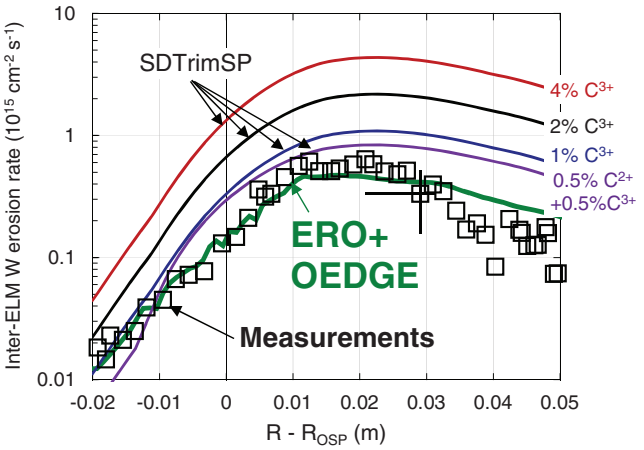

Figure 10. Spectroscopic measurements of the inter-ELM W erosion rate as a function of radial position for the same discharge. The horizontal error bar represents EFIT uncertainty in the OSP position. ERO predictions are overlaid, displaying good agreement with experiment. Predictions from a SDTrimSP sputtering model, also overlaid, are generally higher than the experimental values.

local PMI processes, including physical/chemical sputtering, reflection, and deposition. The second portion tracks test particles ejected from the material surface. Ejected particles begin as neutrals, but once ionized are treated with the full Lorentz force equation, i.e. taking into account the gyromotion of ions. Particles are tracked until they re-deposit on the surface or leave the simulation zone. The version of ERO utilized at DIII-D incorporates a C/W homogenous mixed-material (HMM) model, described in [26] for the W/Be system, to simulate the effective reduction of W erosion in the DIII-D divertor due to effective dilution of the W areal density present on the plasma-facing surface. More details concerning the HMM model are discussed in [9, 27] for the specific case of a C/high-Z system present in the DIII-D divertor. It should be noted that in some cases the ERO-HMM has been unable to reproduce experimental results and more elaborate descriptions of the surface layer (BCA-based, depth-resolved models) have been utilized instead [28], although not brought into routine use with ERO.

Previous studies have indicated that for a 1% concentration of C^{3+} in the edge plasma, the C fraction in the surface interaction layer is approximately 30%, effectively reducing high-Z erosion by 30% [9]. Physical sputtering yields are obtained from the Eckstein database with the Eckstein fit [29] and chemical erosion yields are obtained via the empirical Roth formula [30]. The ERO sputtering database assumes normal incidence for impacting ions, but the difference in C→W sputtering yields between normal and 45° incidence is only ~20% in this low ion impact energy regime. Prompt processes are included in the calculations and results in a ~10% enhancement at the peak of the W erosion profile. The predicted W erosion rate calculated via ERO+OEDGE is shown in figure 10.

To benchmark this ERO prediction, spatially resolved WI emission was measured for this discharge (163216) using the fast filtered camera diagnostic described in section 2.2. WI intensity (photons cm^{-2} s^{-1}) values measured on each pixel were binned in ~0.5 cm radial increments and 100 ms time bins to reduce measurement noise and are again multiplied by the empirical S/XB coefficients, as discussed in section 3 above and in [2], to produce W erosion rates. It should be noted that 3D PMI processes such as the angular distribution of sputtered W atoms (and their finite ionization length) results in an effective 'smearing' of the WI emission profile. A full 3D treatment of these effects would require significant additional effort. However, it is not necessary to develop synthetic diagnostic emission profiles with ERO for neutral W emission because the ionization mean free path (MFP) of these W atoms is very short (~1 mm) and the spatial resolution of the filtered camera is very high (~1 mm) relative to the gradient scale length of the WI emission profile in the radial direction (>10 mm). Thus WI emission is strongly localized near the target surface and the camera captures the true emission profile with minimal smearing due to the finite ionization MFP effect. Experimentally measured W erosion rates are plotted in figure 10 as a function of major radius relative to the OSP position. Because the ELM frequency was ~30 Hz during this discharge, the 100 Hz framing rate of the camera was also sufficient to capture a number of frames without ELMs, allowing the inter-ELM component of the W erosion rate to be extracted. The OSP was swept slowly inboard and outboard across DiMES to build up the complete inter-ELM W erosion profile. A 0.8 cm radial shift (within the uncertainty of the magnetic reconstruction) has been applied to the measured

data to match the peak of the predicted and measured W erosion profiles.

The ERO simulations reproduce well both the shape and magnitude of the experimentally measured W erosion profile within the error bars of the measurement. The ERO model shows good agreement with data over a T_e range of ~7 eV in the PFR to ~35 eV at the peak of the W erosion profile. As noted above, a crucial feature of the ERO code is the C/W mixed-material model, which accounts for the effective reduction of the erosion rate of a high-*Z* surface due to high-*Z*/low-*Z* material mixing. These results imply that W source rates during the inter-ELM phase of DIII-D can be reasonably explained via impurity-induced C→W sputtering using ERO+OEDGE. Certainly it is possible that there are additional PMI physics effects at play and that agreement between and experiment and model is simply fortuitous in this case. However, it good agreement is achieved here in part due to extensive efforts to characterize the divertor plasma parameters and C/W impurity radiation profiles as accurately possible; such extensive measurements were often not available in previous studies on other devices.

This level of agreement can be contrasted with the SDTrimSP sputtering model, also shown in figure 10. Note that cubic spline interpolation, rather than the linear interpolation used by the OEDGE code, has been applied to the D ion flux profile in figure 7(*a*) to produce the SDTrimSP profiles in figure 10. This results in somewhat 'smoother' inferred W erosion profiles for the SDTrimSP cases relative to the ERO+OEDGE case. While the simple sputtering model provides order of magnitude level agreement, it cannot reproduce all features of the W erosion curve over this broad range of electron temperatures. Using a similar C impurity flux profile to that produced by OEDGE (0.5% C^{2+} and 0.5% C^{3+}) results in an under-estimation of the W erosion rate in the PFR and an over-estimation in the CFR.

6. Discussion and conclusions

In this paper, the first spectroscopic measurements of the L-mode and inter-ELM H-mode W erosion profiles in DIII-D are described. This represents a notable extension of previous high-*Z* erosion measurements conducted via DIII-D/DiMES, which have only been inferred via post-mortem analysis after plasma exposures to constant L-mode conditions. Similarly, ERO has previously only been benchmarked against measured W erosion rates on DIII-D [9] using constant L-mode conditions, no spatial resolution, and using C impurity concentrations as free parameter. On ASDEX-U, the ERO code has previously shown reasonably good agreement with post-mortem measurements of net erosion in H-mode from a W-coated C limiter [10], but with several free parameters due to poorly characterized background plasma conditions. On JET-ILW, ERO has been utilized to benchmark spectroscopic measurements of the gross erosion of Be limiters [11]; agreement between code and experiment is observed within the uncertainties associated with plasma conditions and Be S/XB coefficients.

In fact the largest source of uncertainty on the W erosion source in the DIII-D or any tokamak divertor/limiter is the absolute value of the S/XB coefficients. The results in section 3 of this work demonstrate that a simple empirical scaling that is only a function of electron temperature is not sufficient to capture the changes in the S/XB ratio that occur as the electron density increases beyond 10^{13} cm^{-3}. During full or partial detachment on DIII-D and other machines, n_e always lies significantly above this threshold. In addition, transient increases in n_e also occur during edge localized modes (ELMs), so using the empirical scaling of [2] will underestimate the W erosion source during ELMs. Further atomic physics modeling efforts must be undertaken in order to resolve the existing discrepancies between measurement and theoretical modeling. Determining S/XB coefficients from theory involves the calculation of ionization rates, photon emissivity coefficients and branching ratios, all of which pose modeling challenges. The physics assumptions underlying each calculation set should be further analyzed for validity. A thorough discussion of the merits of the different methods used in [5, 22] is beyond the scope of this paper, but it can be noted that the ionization data set used by ERO is obtained from [22] and calculated W re-deposition fractions in the DIII-D divertor agree fairly well with experiment [9]. At present it is concluded that the error bars of 50% on the WI 400.9 nm S/XB ratio determined in [2] are appropriate, particularly for $n_e > 10^{13}$ cm^{-3}.

We also acknowledge that this paper does not present measurements or modeling of the W erosion source during transient events. It has been shown that during attached H-mode conditions on JET, the intra-ELM W erosion source dominates the inter-ELM source, and the magnitude of these intra-ELM erosion rates are fairly consistent with energetic D→W sputtering [31]. A similar analysis is underway for intra-ELM W erosion data from DIII-D and the results will be presented in a subsequent paper. The goal of these studies is to enhance the spatial resolution of H-mode W erosion measurements and perform parameter scans to benchmark models and therefore aid the development of predictive capabilities. Erosion of W material has also been observed via unipolar arcing events on W-coated DiMES samples [32], which in attached H-mode discharges is sometimes comparable to greater than the W impurity source induced via sputtering.

Finally, while this study focuses on the gross erosion rate of tungsten, prompt W redeposition is also an important factor governing the overall W leakage from the divertor region. No measurements of WII emission were acquired in these experiments, so no spectroscopic estimates of prompt W redeposition [2] were available. However, prompt W re-deposition has been investigated extensively via post-mortem analysis techniques in DIII-D L-mode experiments [13]. A prompt W redeposition fraction of 0.53 was measured at a divertor density of 1.6×10^{13} cm^{-3}, and this ratio increased to 0.74 for $n_e = 4.5 \times 10^{13}$ cm^{-3}. These results were in fair agreement with ERO [33] and WBC-REDEP [23] simulations, respectively, and are also qualitatively consistent with a decrease in the W ionization mean free path at higher electron density leading to a higher prompt W redeposition fraction.

The main conclusion of this paper is that detailed measurements of the inter-ELM tungsten erosion source and plasma conditions in tokamak divertors must be performed with high spatial resolution in order to be properly benchmarked against PMI models. A simple semi-analytic PMI model based on SDTrimSP calculations, while capturing the general trends associated with W erosion in the divertor, does not accurately capture the spatial variation of the W erosion profile. A realistic 3D model of the complete PMI picture should be incorporated, including a full main ion and impurity plasma background from a 2D impurity transport code such as OEDGE and a 3D Monte Carlo, mixed-material PMI model such as ERO. Further code benchmarking should focus on reconstructing more gross erosion profiles on high-Z tokamak divertor surfaces. Net erosion profiles should also be inferred via line ratio spectroscopy or other methods; see [2] for some preliminary work on this topic. Most importantly, 3D PMI models of the intra-ELM high-Z erosion source should be developed to aid the understanding of high-Z erosion as a function of ELM frequency, amplitude, and ion flux distribution to the target.

Acknowledgments

This work was supported by U.S. DOE under DE-FC02-04ER54698, DE-FG02-07ER54917, DE-SC00019691, DE-AC52-07NA27344, DE-AC05-00OR22725, and DE-AC04-94AL85000. This material is based upon work supported by the US Department of Energy, Office of Science, Office of Fusion Energy Sciences and Office of Advanced Scientific Computing Research through the Scientific Discovery through Advanced Computing (SciDAC) project on Plasma-Surface Interactions, under Award No. GA-DE-SC0008698. This author would like to thank Prof Stuart Loch and Dr Sebastijan Brezinsek for valuable discussions and contributions.

References

[1] Loarte A. *et al* 2014 *Nucl. Fusion* **54** 033007
[2] van Rooij G.J. *et al* 2013 *J. Nucl. Mater.* **438** S42
[3] Den Harder N. *et al* 2016 *Nucl. Fusion* **56** 026014
[4] Dux R. *et al* 2009 *J. Nucl. Mater.* **390–1** 858
[5] Brezinsek S. *et al* 2013 The JET-ILW and plasma edge spectroscopy in metallic fusion devices *18th Int. Conf.: Atomic Processes in Plasmas (Auburn, USA, 7–10 October 2013)*
[6] Summers H.P. 2004 *The ADAS User Manual, version 2.6* www.adas.ac.uk
[7] Elder J.D., Stangeby P.C., Abrams T., Ding R., Leonard A.W., McLean A.G., Rudakov D.L., Unterberg E.A. and Watkins J.G. 2017 *Nucl. Mater. Energy* accepted
[8] Kirschner A., Philipps V., Winter J. and Kögler U. 2000 *Nucl. Fusion* **40** 989
[9] Ding R. *et al* 2016 *Nucl. Fusion* **56** 016021
[10] Karhunen J., Airila M.I., Hakola A., Herrmann A., Mayer M., Müller H.W., Neu R. and Rhode V. 2012 Discharge-resolved erosion processes at the low-field side midplane of ASDEX upgrade *Proc. 39th EPS on Plasma Physics (Stockholm, Sweden, 2–6 July 2012)* (http://ocs.ciemat.es/EPSICPP2012PAP/pdf/P1.084.pdf)
[11] Borodin D. *et al* 2016 *Nucl. Mater. Energy* **9** 604
[12] Wong C.P.C. *et al* 1992 *J. Nucl. Mater.* **196–8** 871
[13] Rudakov D.L. *et al* 2014 *Phys. Scr.* **T159** 014030
[14] Laengner M. *et al* 2013 *J. Nucl. Mater.* **438** S865
[15] Brooks N.H., Howald A., Klepper K. and West P. 1992 *Rev. Sci. Instrum.* **63** 5167
[16] Colchin R.J., Hillis D.L., Maingi R., Klepper C.C. and Brooks N.H. 2003 *Rev. Sci. Instrum.* **74** 3
[17] Unterberg E.A. *et al* 2016 Fast spectroscopic measurements of tungsten neutral flux due to plasma-material interactions using a two-filter, fiber-optic coupled diagnostic in the DIII-D divertor *21st High-Temperature Plasma Diagnostics Conf. (Madison, USA, June 2016)*
[18] Watkins J.G., Labombard B., Stangeby P.C., Lasnier C.J., McLean A.G., Nygren R.E., Boedo J., Leonard A.W. and Rudakov D.L. 2015 *J. Nucl. Mater.* **463** 436
[19] McLean A.G. *et al* 2016 The Role of Drifts and Radiating Species in Detached Divertor Operation at DIII-D *Preprint: 2016 IAEA Fusion Energy Conf. (Kyoto, Japan, 17–22 October 2016)* (https://conferences.iaea.org/indico/event/98/session/9/contribution/369/material/slides/0.pdf)
[20] Pospieszczyk A. *et al* 2010 *J. Phys. B: At. Mol. Opt. Phys.* **43** 144017
[21] Nishijima D., Doerner R.P., Baldwin M.J., Pospieszczyk A. and Kreter A. 2011 *Phys. Plasmas* **18** 019901
[22] Beigman I., Pospieszczyk A., Sergienko G., Yu Tolstikhina I. and Vainshtein L. 2007 *Plasma Phys. Control. Fusion* **49** 1833
[23] Brooks J.N., Elder J.D., McLean A.G., Rudakov D.L., Stangeby P.C. and Wampler W.R. 2015 *Fusion Eng. Des.* **94** 67
[24] Hofsäss H., Zhang K. and Mutzke A. 2014 *Appl. Surf. Sci.* **310** 134
[25] Stangeby P.C. *et al* 2003 *J. Nucl. Mater.* **313–6** 883
[26] Kirschner A. *et al* 2009 *J. Nucl. Mater.* **390–1** 152
[27] Guterl J., Abrams T., Ding R., Guo H.Y. and Rudakov D.L. 2017 *Nucl. Mater. Energy* submitted
[28] Droste S., Kirschner A., Borodin D., Kreter A., Brezinsek S., Philipps V., Samm U. and Schmitz O. 2008 *Plasma Phys. Control. Fusion* **50** 015006
[29] Behrisch R. and Eckstein W. 2007 *Sputtering by Particle Bombardment* (Berlin: Springer)
[30] Roth J. *et al* 2005 *J. Nucl. Mater.* **970** 337
[31] Guillemaut C. *et al* 2016 *Phys. Scr.* **T167** 014005
[32] Rudakov D.L., Chrobak C.P., Doerner R.P., Krasheninnikov S.I., Moyer R.A., Umstadter K.R., Wampler W.R. and Wong C.P.C. 2013 *J. Nucl. Mater.* **438** S805
[33] Ding R. *et al* 2017 *Nucl. Mater. Energy* (https://doi.org/10.1016/j.nme.2017.03.012)